Optimization of the Surface Structure of Heating Filaments With Regard to Their Apparent Thermal Emissivity

B. Valentini*, A. Plankensteiner*

* PLANSEE SE, 6600 Reutte, Austria

Abstract

High-temperature furnaces are typically heated by refractory metal based resistive heaters of filament, wire or sheet shape, respectively. The heaters are typically located in close range to sinter ingots and are enclosed by the thermal insulation of the furnace thus transferring heat in almost equal parts to sinter ingots and the insulation via radiation and convection. In case of low-pressure or vacuum furnaces thermal radiation is the predominant heat transfer mechanism and consequently the heat flux from the heaters to their environment depends, according to Stefan-Boltzmann's law, on emissivities and absolute temperatures of all involved surfaces. Hence, increasing apparent thermal emissivities of heater surfaces facing sinter ingots lead to more pronounced inward-directed heat transfer and reduced heater temperatures. As analytically and experimentally shown by Psarouthakis in 1963, the apparent thermal surface emissivity, here the inward heater surface, increases by superficial structures. In the present contribution, the thermo-electrical coupled system of a resistive sheet-heater with a one-sided superficial structure of various morphologies is investigated by numerical simulations aiming at maximizing the apparent thermal emissivity.

Keywords

Thermal emissivity, apparent thermal emissivity, thermal radiation, surface structure, heating filament, refractory metal, finite element analysis

Introduction

High temperature furnaces and reactors with corresponding hot zones enclosing the operational space typically make use of refractory metal based heating elements and thermal shielding systems, see Fig. 1. Most of these furnaces are driven by resistive heating elements. The thermal surface properties of the heating elements at their respective inward and outward side strongly influence the required temperatures of the heater elements, thus, influencing the energy consumption required for the underlying process. Since the furnace atmosphere has to be vacuum or of protective, i.e., non-oxidizing, type heating elements made of refractory metals keep their dense, smooth and clean surfaces over a long time operational which is accompanied with an unaltered and intrinsically low thermal emissivity. Therefore, it is of primary practical importance to evaluate potential surface modifications aiming at

increasing the apparent thermal emissivity of the surface of the heating elements preferably at the inward side only. As analytically and experimentally shown in [1], the apparent thermal surface emissivity can be increased by superficial structures. Hence, in the present contribution various morphologies of superficial structures are compared to each by applying numerical simulations.

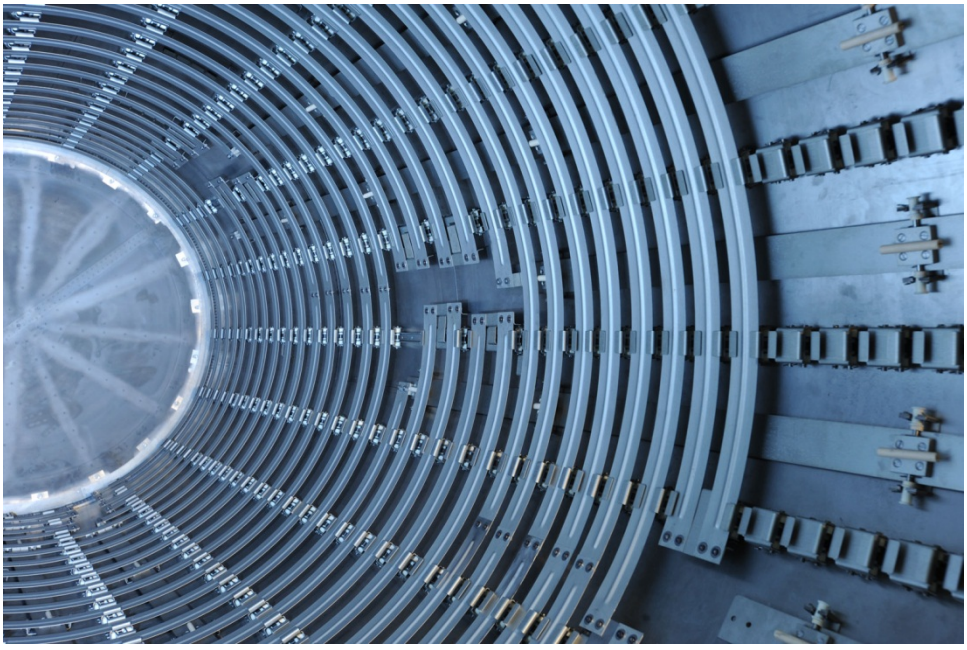

Figure 1: Hot zone of a circular furnace with meandering heater system.

The materials used in high temperature furnaces are regularly subjected to extreme thermal and mechanical loading as well as harsh chemical environments. Refractory metals such as molybdenum and tungsten as well as their alloys are capable to withstand these damaging conditions. Additionally, they exhibit many advantageous properties as high melting points permitting operational temperatures up to about $2800\ [°C]$, excellent high-temperature strengths for thin-walled component designs, low heat capacity for rapid transient thermal behavior, low coefficient of thermal expansion for low thermal induced strains and stresses, and dense metallic surfaces avoiding absorption of gases representing some of the important ones. Molybdenum and tungsten also exhibit a fairly good machinability and are available, e.g., as semi-finished products such as sheets, bars and wires. For instance, in the photovoltaic and LED industry molybdenum and tungsten are typically used for all parts within the hot zone of high temperature furnaces for consolidation and crystal growth purposes or in the coating industry for high temperature reactors. Such furnaces and reactors are operated at temperatures of $2000\ [°C]$ and above. Hence, within the furnaces and reactors the hot zones require an adequate thermal insulation, e.g., a thermal radiation shield system. Heating elements are also found in sintering furnaces as they are used for the powder metallurgical production route where high temperature furnaces of resistive heating type are typically employed. Depending on the geometrical dimensions of the sintering part different sizes of furnaces and heaters are used. In case of the sintering of refractory metals typical dimensions of cylindrical heating elements are up to about $900\ [mm]$ in diameter and $1800\ [mm]$ in height typically made from thin-walled tungsten sheet material.

Mathematical Description of Resistive Heating

From a physical point of view resistive heating is described by Joule's law which states proportionality of the heat Q $[J]$ produced in a resistive device to the electrical power p $[VA = W]$ applied to it integrated over the time interval $\Delta t = [t_1, t_2]$ $[s]$:

$$Q = \int_{t_1}^{t_2} p(\boldsymbol{x}, t)\, dt \tag{1}$$

The electrical power depends on the coordinate $\boldsymbol{x}$ $[m]$ and on the time $[s]$. For the general case of alternating current the electrical power for an arbitrary transient electrical current is given as (see, e.g. [2])

$$p(\boldsymbol{x}, t) = u(\boldsymbol{x}, t)\, i(\boldsymbol{x}, t) \tag{2}$$

with u $[V]$ and i $[A]$ representing the spatial- and time-dependent voltage and electrical current, respectively. The electrical voltage in (2) is defined as the difference of the electrical potential φ_e $[V]$ between two points P_1 and P_2:

$$u(\boldsymbol{x}, t) = \varphi_e(\boldsymbol{x}, t)|_{P_1} - \varphi_e(\boldsymbol{x}, t)|_{P_2} = \int_{P_1}^{P_2} \vec{\boldsymbol{E}}(\boldsymbol{x}, t) \cdot d\vec{\boldsymbol{s}} \tag{3}$$

where $\vec{\boldsymbol{E}}$ $[V/m]$ is the spatial- and time-dependent vector of electrical field intensities and $d\vec{\boldsymbol{s}}$ $[m]$ the path of integration. With the aid of Ohm's law (in differential form)

$$\vec{\boldsymbol{j}}(\boldsymbol{x}, t) = \tilde{\boldsymbol{\kappa}}(\boldsymbol{x}, t) \cdot \vec{\boldsymbol{E}}(\boldsymbol{x}, t) \tag{4}$$

the electrical current is derived from the electrical field intensity as

$$i(\boldsymbol{x}, t) = \iint_A \vec{\boldsymbol{j}}(\boldsymbol{x}, t) \cdot d\vec{\boldsymbol{A}} = \iint_A \left(\tilde{\boldsymbol{\kappa}}(\boldsymbol{x}, t) \cdot \vec{\boldsymbol{E}}(\boldsymbol{x}, t)\right) \cdot d\vec{\boldsymbol{A}}. \tag{5}$$

In (4) $\vec{\boldsymbol{j}}$ $[A/m^2]$ and $\tilde{\boldsymbol{\kappa}}$ $[1/(\Omega \cdot \mathrm{m})]$ denote the vector of electrical current densities and the second-order tensor of electrical conductivities of an anisotropic material, respectively. Actually, the tensor of electrical conductivities also depends on the current temperature. In case of an isotropic material the tensor of electrical conductivities reduces to $\tilde{\boldsymbol{\kappa}} = \kappa \tilde{\boldsymbol{\delta}}$ with the scalar κ representing the electrical conductivity in each direction of the material and $\tilde{\boldsymbol{\delta}}$ the Kronecker delta. The integral in (5) is performed over the vector area $\vec{\boldsymbol{A}}$ $[m^2]$. Inserting (2), (3) and (5) in (1) results into

$$\begin{aligned} Q &= \int_{t_1}^{t_2} \iiint_V \left(\tilde{\boldsymbol{\kappa}}(\boldsymbol{x}, t) \cdot \vec{\boldsymbol{E}}(\boldsymbol{x}, t)\right) \cdot \vec{\boldsymbol{E}}(\boldsymbol{x}, t) dV dt = \\ &= \int_{t_1}^{t_2} \iiint_V \left(\tilde{\boldsymbol{\varrho}}_R(\boldsymbol{x}, t) \cdot \vec{\boldsymbol{j}}(\boldsymbol{x}, t)\right) \cdot \vec{\boldsymbol{j}}(\boldsymbol{x}, t) dV dt \end{aligned} \tag{6}$$

where $\tilde{\boldsymbol{\varrho}}_R = \tilde{\boldsymbol{\kappa}}^{-1}$ $[\Omega \mathrm{m}]$ is the second-order tensor of electrical resistivities and V $[m^3]$ the volume which is heated resistively. The electrically induced heat given in (6) defines the source-term for the thermal situation – involving thermal conductance, convection, advection and radiation – to be solved.

Mathematical Description of Thermal Radiative Heat Transfer

Since heat transfer at high temperatures under vacuum or almost vacuum conditions is primarily driven by thermal radiation – thermal conductance and convection are assumed to be negligible – the mathematical theory of radiative heat transfer is described briefly and, thus, not exhaustively in the following. A more complete description can be found, e.g., in [3] or [4]. The flux of energy radiation from a black body depends strongly on the absolute temperature of the body and on the wavelength of the emitted radiation (Planck's law). The total flux of energy radiation from the black body $e_b\ [W/m^2]$ can be described mathematically by the Stefan-Boltzmann law which is written as

$$e_b(T) = \sigma T^4. \tag{7}$$

In (7) $\sigma = 5.6704 \cdot 10^{-8}\ [W/(m^2 \cdot K^4)]$ denotes the Stefan-Boltzmann constant and $T\ [K]$ names the temperature in the Kelvin scale (absolute temperature) which is related to the temperature in the Celsius scale $\theta\ [°C]$ by $T = \theta - \theta_0$ with the temperature at absolute zero defined as $\theta_0 = -273.15\ [°C]$. The radiative behavior of a real body is different to that of a black body inasmuch as that the total flux of energy emitted from a real body is usually lower than those emitted form a black body, i.e., $e_{rb}(T) \leq e_b(T)$. In addition, the emitted flux of energy varies with wavelength of the radiation and depends on the angle at which the radiation is emitted. However, in numerous engineering applications the thermal behavior of a real body can be approximated in a sufficiently accurate way by the behavior of a so-called diffuse, gray body. In the context of thermal radiation a body is called diffuse if its emittance (absorbance) is independent of the angle at which the radiation is emitted (absorbed). Furthermore, the body is called gray if its emittance (absorbance) has no wavelength dependency on the emitted (absorbed) thermal radiation. Hence, the emittance of the diffuse, gray body $0 < \varepsilon \leq 1\ [-]$ is given as the ratio of the total heat flux emitted from a diffuse, gray body $e_{gb}(T)\ [W/m^2]$ and a black body (7):

$$\varepsilon(T) = \frac{e_{gb}(T)}{e_b(T)} = \frac{e_{gb}(T)}{\sigma T^4}. \tag{8}$$

According to Kirchhoff's law for a diffuse, gray body the absorbance $\alpha\ [-]$ of the body is equal to its emissivity:

$$\alpha(T) = \varepsilon(T). \tag{9}$$

Conservation of energy requires that the total incident energy upon a body is either partially/completely absorbed, reflected and/or transmitted, respectively. Thus, the sum of the absorbance, reflectance $\varrho\ [-]$ and transmittance $\tau\ [-]$ must be equal to one:

$$\alpha(T) + \varrho(T) + \tau(T) = 1. \tag{10}$$

Consequently, assuming the body to be opaque, i.e., $\tau = 0$, and inserting (9) in (10) the reflectance of an opaque, diffuse, gray body is gained as

$$\varrho(T) = 1 - \varepsilon(T). \tag{11}$$

Since a diffuse body emits heat into its environment independently of the angle, the fraction of heat emitted from the surface of an isothermal, diffuse body i to another isothermal, diffuse body j is computed as

$$F_{i\to j} = \frac{1}{A_1\pi}\int_{A_1}\int_{A_2}\frac{\cos(\beta_1)\cos(\beta_2)}{s^2}dA_2dA_1 \tag{12}$$

where $A_1\ [m^2]$ and $A_2\ [m^2]$ denote the areas of the bodies i and j, respectively, and $s\ [m]$ is the distance between the infinitely small areas $dA_1\ [m^2]$ and $dA_2\ [m^2]$. In (12) the angles $\beta_1\ [°]$ and $\beta_2\ [°]$, respectively, are defined as the angle between the surface normal of the respective infinitely small area and the line connecting the (centers of the) infinitely small areas. $F_{i\to j}$ in (12) is called view factor, configuration factor or shape factor ([3]). Conservation of energy requires that for each surface $i = 1,\dots,m$ the sum of all fractions $F_{i\to j}, j = 1,\dots,n$ has to equal to one, i.e.,

$$F_{i\to 1} + F_{i\to 2}+\dots+F_{i\to i}+\dots+F_{i\to j}+\dots+F_{i\to n} = 1. \tag{13}$$

Making use of the view factor reciprocity

$$A_iF_{i\to j} = A_jF_{j\to i} \tag{14}$$

the net heat flux $q_{i\to j}\ [W/m^2]$ transferred from body i to body j is derived as (see e.g. [3] or [4])

$$q_{i\to j}(T_i,T_j) = \sigma\frac{\left(T_i^4-T_j^4\right)}{A_i\left(\frac{1-\varepsilon_i}{\varepsilon_iA_i}+\frac{1}{A_iF_{i\to j}}+\frac{1-\varepsilon_j}{\varepsilon_jA_j}\right)}. \tag{15}$$

where the emittances of the two bodies are assumed to be independent of the temperatures at the surface of the bodies, i.e., $\varepsilon_i = const.$ and $\varepsilon_j = const.$. In case of two diffuse, gray, and infinite bodies $i = 1$ and $j = 2$ with parallel surfaces the net heat flux is computed with $F_{1\to 2} = 1$ from (16) as

$$q_{1\to 2}(T_1,T_2) = \sigma\frac{\left(T_1^4-T_2^4\right)}{\frac{1}{\varepsilon_1}+\frac{1}{\varepsilon_2}-1}. \tag{16}$$

From (16) and (17), respectively, the total net heat flux transferred from body i to body j is

$$Q_{i\to j}(T_i,T_j) = q_{i\to j}(T_i,T_j)A_i. \tag{17}$$

Comparison of the Apparent Emissivity of a Superficially Structured Surface with Prisms

In this section a comparison of the apparent thermal emissivity of superficially structured surfaces is presented ([5]). To this end one surface of a cuboid representing, e.g., a heating filament is enhanced by a superficial structure assembled of a series of cuboids arranged periodically in two orthogonal directions. In the following the former, underlying cuboid will be denoted as “base” and the assembly of cuboids representing the superficial structure will be named “structure”. The impact of the topology of the structure on the apparent thermal emissivity is studied by varying the aspect ratio of the cuboids and the distance between the cuboids. However, for each variation of the structure the aspect ratio of all cuboids and the distance of all cuboids to each other, respectively, are assumed to be the constant. It is worth noting that the dimensions of the structure are assumed to be considerably larger than the wavelength of the thermal radiation. The apparent thermal emissivity of each superficially structured surface is

computed on the basis of finite element analyses. All numerical simulations presented in the present contribution are carried out with the finite element program ABAQUS 6.12-1 [6].

Finite Element Model

Due to the periodical assembly of the structure in two orthogonal directions only one unit cell containing one cuboid of the superficial structure and one prismatic part of the base is considered in the numerical simulations, see Fig. 6a. The thermal radiative behavior of the whole assembly (actually an assumed assembly of infinite number of cuboids) is approximated by applying a finite number of periodic symmetry conditions in each direction at the lateral faces of the unit cell, respectively. The number of periodic symmetries at the lateral face and in each direction, respectively, is chosen as five. Consequently, the thermal radiative interaction between the unit cell in the center of the assembly and the $(2 \cdot 5 + 1)^2 - 1 = 120$ surrounding unit cells, considered by the period symmetry conditions, is accounted for in the numerical models. In all numerical models the height of the base is defined as $h_1 = 0.10\ [mm]$ and the width and length of the cuboid of the structure are fixed as $a_2 = 0.40\ [mm]$. The height of the cuboid h_2, the distance between the cuboids in both orthogonal directions b and the width and length of the base $a_1 = a_2 + b$ are defined as a function of a_2. The aspect ratios of h_2/a_2, b/a_2 and a_1/a_2, respectively, investigated in the numerical models are summarized in Table I. Exemplarily, Fig. 6b shows the finite element mesh of the variant with $h_2/a_2 = 1$ and $b/a_2 = 0.5$. The approximate length of the edges of the finite elements is chosen as $a_1/20$.

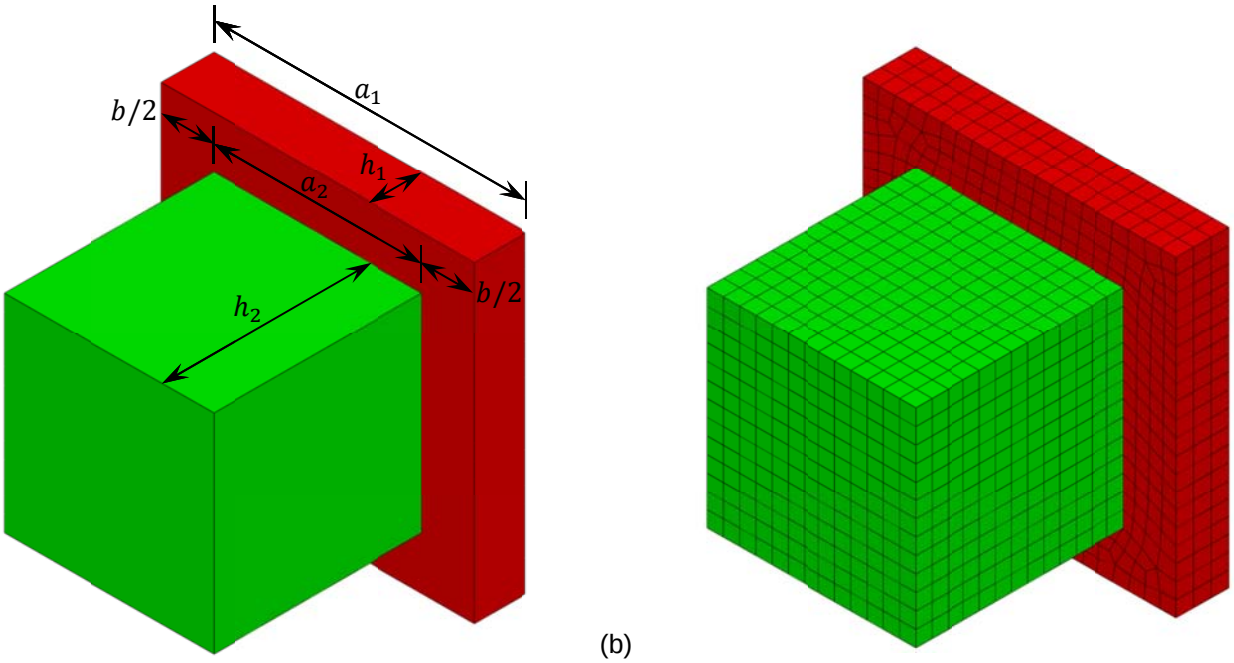

(a) (b)

Figure 6: Unit cell of the superficially structured surface with $h_2/a_2 = 1$ and $b/a_2 = 0.5$: (a) geometry with dimensions and (b) finite element mesh; prismatic base (red) and prismatic superficial structure (green).

Table I: Aspect ratios of the cuboids used in the numerical models of the unit cell

h_2/a_2	b/a_2	a_1/a_2
$[-]$	$[-]$	$[-]$
$[0.001, 0.25, 0.50, 1, 2, 3, 4, 6, 8, 10]$	$[0.25, 0.50, 1, 2]$	$[1.25, 1.50, 2, 3]$

Boundary Conditions

In all numerical models the temperature at all nodes of the base and the structure is defined as $\theta_{surf} = 1000\ [°C]$. The prescribed temperature is kept constant during the whole computation. Hence, no heat flux due to thermal conduction takes place and all material parameters except the emissivity of the surface are of no relevance to the considered results of the numerical simulations. At the structured side of the unit cell a thermal radiation boundary condition to a constant ambient temperature of $\theta_{amb.} = 20\ [°C]$ is applied. For each geometrical variant the emissivity of the whole surface is varied with discrete values of the emissivity of $\varepsilon = [0.2,\ 0.4,\ 0.6,\ 0.8,\ 1.0]$. The rear face and the four lateral faces of the base are assumed to be perfectly insulated. Consequently, only heat is emitted from the superficially structured surface to the ambient space.

Computation of the Apparent Thermal Emissivity

The heat flux emitted from a black body ($\varepsilon = 1$) of area $A = a_1^2$ and temperature θ_{surf} to an ambient temperature $\theta_{amb.}$ is computed with the aid of (16) and (17) as

$$Q_{b,plain} = \sigma\left(T_{surf.}^4 - T_{amb.}^4\right)A = \sigma\left(T_{surf.}^4 - T_{amb.}^4\right)a_1^2 = 148.55\ a_1^2\ [mW/mm^2]. \qquad (18)$$

Making use of (8) the apparent thermal emissivity of a diffuse, gray and superficially structured surface (with dimensions depicted to Fig. 6a) is derived according to [1] as

$$\varepsilon_{app.}(\varepsilon, a_1, \mathrm{b}, h_2) = \left.\frac{Q_{gb,struc.}(\varepsilon, a_1, \mathrm{b}, h_2)}{Q_{b,plain}(a_1)}\right|_{\theta_{surf}, \theta_{amb.}}. \qquad (19)$$

In (19) $Q_{gb,struc.}$ represents the heat flux emitted from a diffuse, gray and superficially structured surface at temperature θ_{surf} to an ambient temperature $\theta_{amb.}$. It has to be pointed out that (19) is only valid if $Q_{b,plain}$ and $Q_{gb,struc.}$ are computed with the same thermal boundary conditions and the projected area under consideration is the same. In the present contribution $Q_{b,plain}$ is derived from (18) and $Q_{gb,struc.}$ is evaluated from the numerical simulations by summation of the heat flux emitted from the superficially structured surface to the ambient boundary condition. Two limiting cases can be derived from (19): Firstly, in case of $\varepsilon \to 1$ the apparent thermal emissivity tends to one, i.e., $\varepsilon_{app.} \to 1$. Secondly, in case of $h_2/a_2 \to 0$ the apparent thermal emissivity tends to the emissivity of the surface, that is, $\varepsilon_{app.} \to \varepsilon$.

Analysis Results

Figure 7 shows the computed apparent thermal emissivities of the superficially structured surface $\varepsilon_{app.}$ plotted over the ratio of height to length of the structure h_2/a_2. The colors of the curves indicate the respective prescribed emissivity of the surface ε and the four line styles represent the assumed ratios b/a_2. The inaccuracy of the predicted apparent thermal emissivities resulting from the finite number of periodic symmetry conditions and finite number of finite elements used in the numerical simulations can be inferred for the limiting case of a black body, i.e., $\varepsilon = 1$. As mentioned above, for $\varepsilon = 1$ the apparent thermal emissivity should become $\varepsilon_{app.}(\varepsilon = 1) = 1$. Hence, the error of the computed apparent thermal emissivities grows with increasing aspect ratio h_2/a_2 and reaches at most $5\ [\%]$ at $h_2/a_2 = 10$. The error of the results computed with $\varepsilon < 1$ is assumed to be about the same size. As can be seen in Fig. 7, in general, the apparent thermal emissivity of the diffuse, gray and superficially structured surfaces is

higher than the emissivity of the surface, i.e., $(\varepsilon_{app.} > \varepsilon)|_{\varepsilon<1}$. The apparent thermal emissivity is strictly increasing with increasing aspect ratio h_2/a_2. The ascent is steepest for small aspect ratios h_2/a_2 and small aspect ratios b/a_2. For small aspect ratios h_2/a_2 a decreasing distance between the cuboids results in an increasing apparent thermal emissivity. With increasing aspect ratio h_2/a_2 a greater distance between the cuboids of the structure leads to an increased apparent thermal emissivity. In Fig. 8 the ratio of the apparent thermal emissivity to the emissivity is plotted over the ratio h_2/a_2. In general it is found that for fixed aspect ratios h_2/a_2 the ratio of the apparent thermal emissivity to the emissivity increases with decreasing emissivity. For instance at fixed aspect ratios $h_2/a_2 = 1$ and $b/a_2 = 0.5$ the ratios the apparent thermal emissivity to the emissivity are predicted as $\varepsilon_{app.}/\varepsilon \approx [1.80, 1.40, 1.20, 1.10]$ for $\varepsilon = [0.20, 0.40, 0.60, 0.80]$, respectively. E.g., the heat emitted by thermal radiation from a structured surface with $\varepsilon = 0.40$ is predicted to be increased by 40 [%] ($\varepsilon_{app.} = 0.56$) compared to a plain surface without any superficial structure.

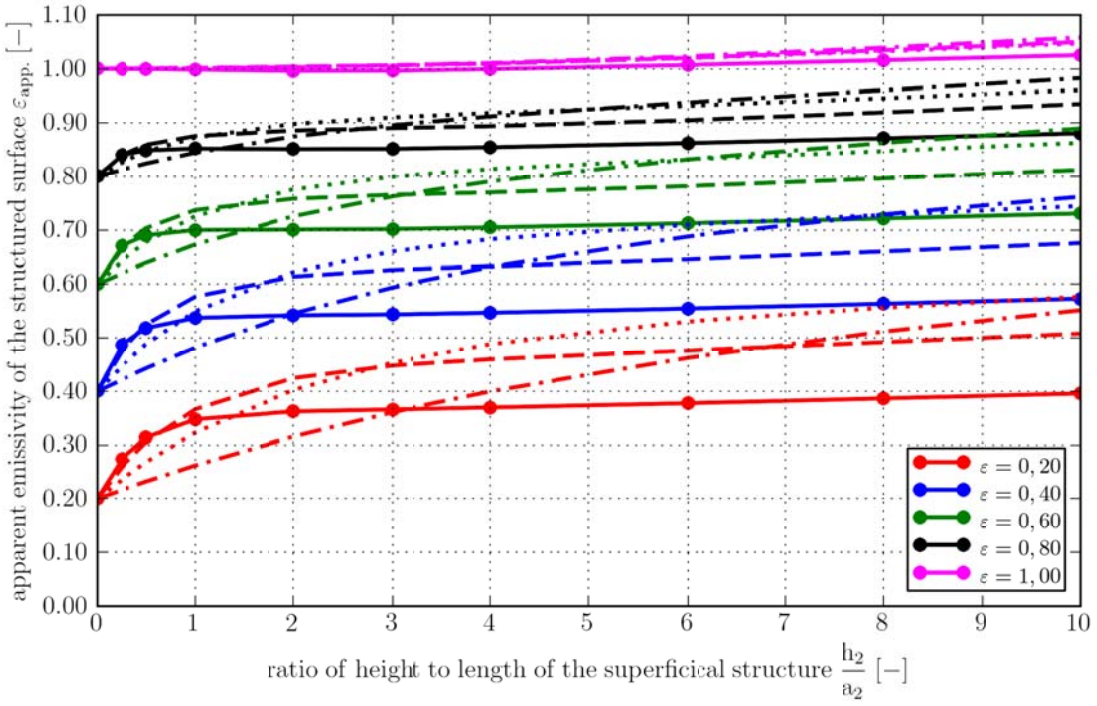

Figure 7: Predicted apparent thermal emissivity of the superficially structured surface in dependence of the slenderness ratio of the individual superficial structural element: solid curves … $b/a_2 = 0.25$; dashed curves … $b/a_2 = 0.50$; dotted curves … $b/a_2 = 1$ and dashed-and-dotted curves … $b/a_2 = 2$.

Numerical Example of a Heating Filament

The applicability of the gained insight in the section above to a heating filament made of tungsten is presented in the following. To this end, the advantage of a superficially structured surface of the heating filament with respect to its thermal radiative behavior is shown by comparing the thermal radiative behavior of two numerical models to each other: i) a plain, unstructured heating filament and ii) a heating filament of the same dimensions but with a superficially structured surface at only one side. In the following the models will be denoted as “plain filament” and “structured filament”, respectively.

Finite Element Model

The examined heating filament has a width of $w = 25\ [mm]$ and a thickness of $t = 1.5\ [mm]$. Its length is assumed to be much larger than its width. Hence, similar to the numerical models in the section above only one prismatic unit cell, shown in Fig. 9a for the case of the structured model, is considered in the numerical models. Figure 9b shows an assembly of 2×11 unit cells representing a short part of the superficially structured heating filament. The unit cell of both models has a length of $l = 1.2\ [mm]$, a thickness t and a width of $w/2 = 12.5\ [mm]$. In case of the finite element model of the superficially structured heating filament the unit cell is enhanced by the periodically arranged structure depicted in Fig. 9a. The dimensions of the structure are chosen as $a_2 = h_2 = 0.8\ [mm]$ and the distance between the cuboids is defined as $b = l - a_2 = 0.4\ [mm]$, i.e, $h_2/a_2 = 1$ and $b/a_2 = 0.5$. The thermal radiative behavior of the whole heating filament is approximated by applying ten periodic symmetry conditions at both sides in longitudinal direction and one reflection symmetry parallel to the longitudinal direction at the plane of symmetry shown in Fig. 9b. Thus, the thermal radiative interaction between the unit cell and the $2 \cdot (2 \cdot 10 + 1) - 1 = 41$ adjacent unit cells is considered in both finite element models.

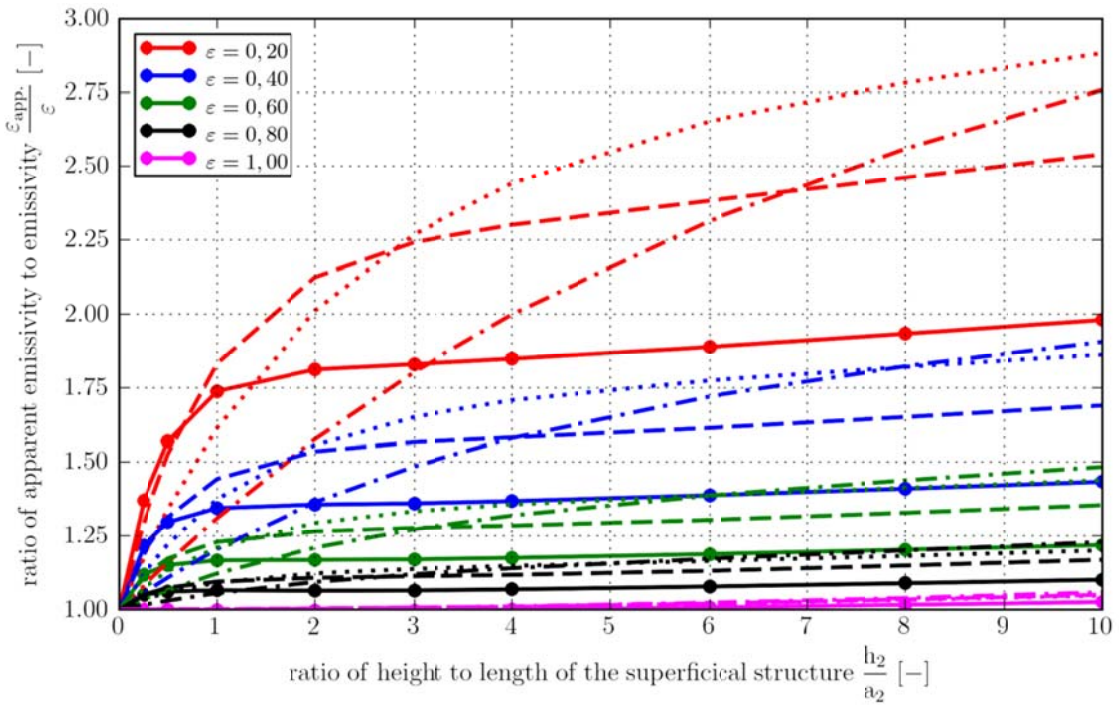

Figure 8: Ratio of the predicted apparent thermal emissivity of the superficially structured surface to the emissivity of the surface in dependence of the slenderness ratio of the individual superfical structural element: solid curves … $b/a_2 = 0.25$; dashed curves … $b/a_2 = 0.50$; dotted curves … $b/a_2 = 1$ and dashed-and-dotted curves … $b/a_2 = 2$.

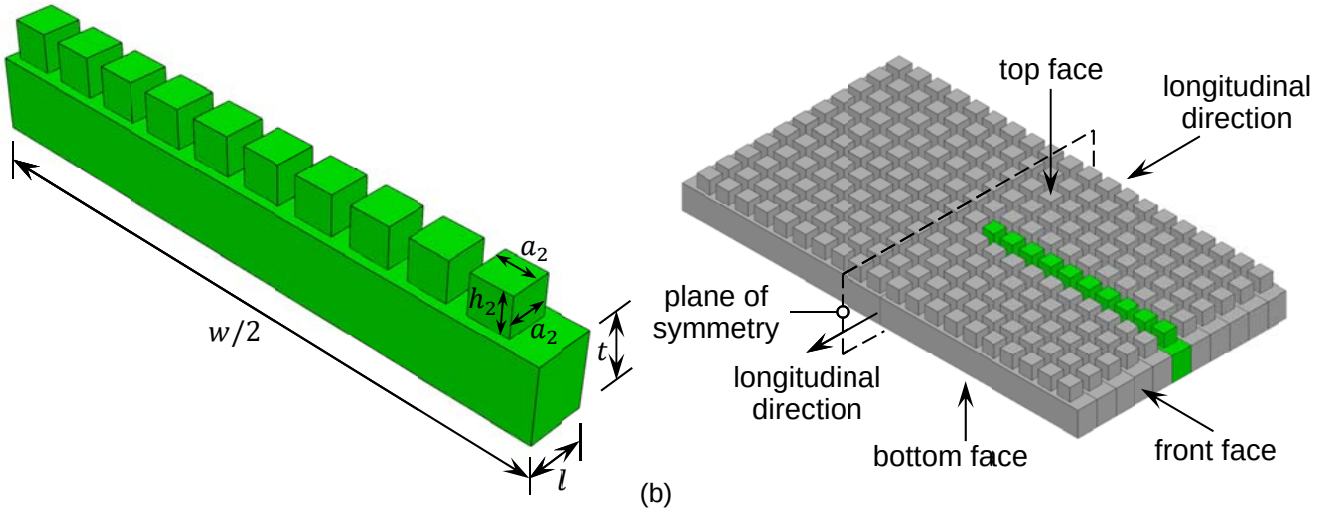

(a) (b)

Figure 9: Geometry of the superficially structured heating filament: (a) unit cell with dimensions and (b) assembly of 2×11 unit cells representing a short part of the heating filament.

Boundary Conditions

In both numerical models the initial temperature at all nodes of the heating filament is chosen as $\theta_{init.} = 1000\ [°C]$. The heating filament is heated resistively by an applied constant electrical current density of $j = 26.67\ [A/mm^2]$ until steady-state conditions are achieved. The resulting temperature at steady-state is predicted to be approximately 1600 to $1700\ [°C]$ with some inhomogeneity depending on the numerical model variant. The electrical current density is applied at the two faces of the unit cell which are orthogonal to the longitudinal direction of the heating filament. At both faces the electrical current density is orientated in the same longitudinal direction. In the plane of the reflection symmetry the electrical potential at only one node is defined as $\varphi_0 = 0\ [mV]$. At all exterior surfaces, i.e., at the top, front and bottom face, respectively, (see Fig. 9b) a thermal radiation boundary condition to a constant ambient temperature of $\theta_{amb.} = 1000\ [°C]$ is applied. The emissivity of all exterior surfaces is defined as $\varepsilon = 0.4$ in both finite element models. In contrast to the computations of the unit cells in the previous section the boundary (front face) of the heating filament also radiates to the ambient space.

Material Parameters

The thermal and electrical material parameters of tungsten used in the numerical models are summarized in Table II. Since the main focus of attention is paid to the radiative behavior of the heating filaments the thermal and electrical material parameters are defined independently of the temperature. However, the values given in Table II are realistic ones for tungsten at a temperature of about $1600\ [°C]$.

Table II: Thermal and electrical material parameters for tungsten used in the numerical models

density	specific heat capacity	thermal conductivity	electrical conductivity
ρ	c_p	λ	κ
$[ton/mm^3]$	$[mJ/(ton \cdot K)]$	$[mW/(mm \cdot K)]$	$[1/(mm \cdot m\Omega)]$
$1.93 \cdot 10^{-8}$	$1.69 \cdot 10^{8}$	125.00	1.80

Analysis Results

The predicted total heat fluxes emitted from the top, bottom and front face, respectively, over a length $l = 1.2\ [mm]$ of the heating filament are summarized in Fig. 10a. For the plain filament the total heat flux computed at the top and bottom face are equal. In contrast, the predicted total heat flux of the structured filament is more pronounced at the top (structured) face than at the bottom (plain) face. I.e., the structured filament is emitting approximately $44\ [\%]$ more energy from the structured face than from the unstructured one which is in good agreement with the result given at the end of the section above. In comparison to the plain filament the structured filament is emitting about $13\ [\%]$ more energy from the top face and circa $21\ [\%]$ less energy from the bottom face. For both models the total heat flux at the front face is significantly lower than the one at the top and bottom face, respectively, because of the smaller area. The total heat flux computed from the sum of the total heat fluxes from the top, bottom and front face results in an about $5\ [\%]$ higher energy output of the plain filament compared to the structured one. This is a result of the lower electrical resistivity of the structured filament compared to the plain filament which in turn results in an approximately $90\ [°C]$ lower maximum and minimum temperature, respectively, within the structured filament. The computed maximum and minimum temperatures of both numerical models are plotted in Fig. 10b and their predicted temperature distribution within the heating filaments is shown in Fig. 11. It is worth mentioning, although the temperature of the structured filament is lower than the one of the plain filament the heat flux on the top surface is still higher in case of the structured filament. Hence, if a structured heating filament is used in, e.g., a high temperature furnace the structured face of the heating filament should be orientated towards, e.g., the sintering ingot and the plain face towards the thermal insulation system, respectively, resulting in a reduced consumption of energy for heating the sintering ingot and an increased life-time of the heating filament because of the reduced average temperature of the filament.

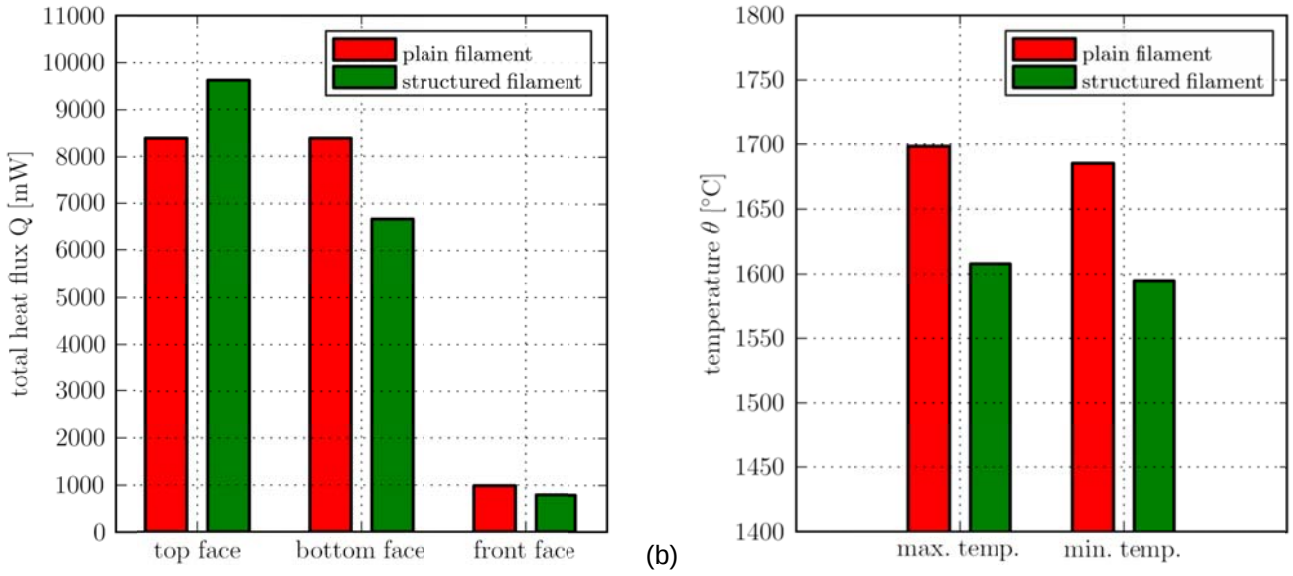

Figure 10: Predicted results of the numerical simulations of a tungsten heating filament: (a) computed total heat flux at the top, bottom, and front face, respectively, over a length $l = 1.2\ [mm]$ of the heating filament and (b) computed maximum and minimum temperatures, respectively, of the whole numerical model; the heat element shows a cross-section of $A = 37.5\ [mm^2]$ with a uniform current density of $j = 26.67\ [A/mm^2]$ being applied.

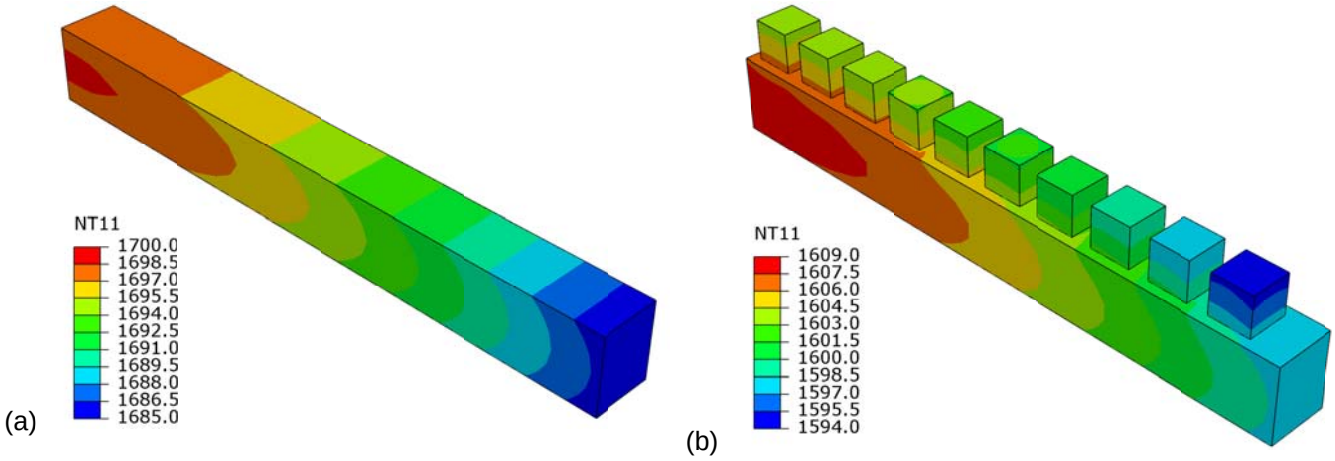

Figure 11: Predicted temperatures of (a) the plain filament and (b) the structured filament both being made of tungsten; the heat element shows a cross-section of $A = 37.5\ [mm^2]$ with a uniform current density of $j = 26.67\ [A/mm^2]$ being applied.

Conclusions

As has been shown by numerical analyses the apparent thermal emissivity of a surface can be increased by enhancing the surface by a superficial structure. The conducted numerical simulations predict that the increase in the apparent emissivity strongly depends on the dimensions of the superficial structure as well as the emissivity of the surface itself. For equally structured surfaces the relative rise of the apparent thermal emissivity increases for decreasing emissivity of the surface. The applicability of such a superficially structured surface has been presented exemplarily by a coupled thermal-electrical finite element analysis of a one-sided superficially structured heating filament. The analysis clearly showed that the structured surface of the heating element emits more heat by radiation than the plain surface, hence, allowing the design of more efficient heaters within, e.g., high temperature furnaces.

References

1. J. Psarouthakis, Apparent Thermal Emissivity from Surfaces with Multiple V-Shaped Grooves, *AIAA Journal*, vol. 1, no. 8, pp. 1879-1882, (1963)
2. M. Albach, *Elektrotechnik*, Imprint der Pearson Education Deutschland GmbH, Munich, Germany, (2011)
3. J.H. Lienhard IV and .H. Lienhard IV, *A Heat Transfer Textbook*, Phlogiston Press, Cambridge, Massachusetts, U.S.A., v. 2.01, (2011)
4. D. Baehr and K. Stephan, *Wärme- und Stoffübertragung*, Springer-Verlag Berlin Heidelberg, (1994)
5. B. Valentini, *Thermische Analysen zur Abhängigkeit der äquivalenten Emissivität einer strukturierten Oberfläche von der Emissivität und Geometrie der Oberfläche*, investigation report, no. IS 3794, PLANSEE SE, Reutte, Austria, 28.01.2013, (2013)
6. *ABAQUS Analysis User's Manual*, Providence, RI, USA, Dassault Systèmes Simulia Corp., (2012)